ADVANCES IN ATMOSPHERIC SCIENCES, VOL. 32, JULY 2015, 909–923

Mid-Pliocene Westerlies from PlioMIP Simulations

LI Xiangyu[1,5], JIANG Dabang*[1,2,3], ZHANG Zhongshi[1,4], ZHANG Ran[3], TIAN Zhiping[3], and YAN Qing[1]

[1]*Nansen–Zhu International Research Centre, Institute of Atmospheric Physics, Chinese Academy of Sciences, Beijing* 100029

[2]*CAS Center for Excellence in Tibetan Plateau Earth Sciences, Beijing* 100101

[3]*Climate Change Research Center, Chinese Academy of Sciences, Beijing* 100029

[4]*UniResearch, Bjerknes Centre for Climate Research, Bergen* 5007, *Norway*

[5]*University of Chinese Academy of Sciences, Beijing* 100049

(Received 8 August 2014; revised 8 November 2014; accepted 2 December 2014)

ABSTRACT

The midlatitude westerlies are one of the major components of the global atmospheric circulation. They play an important role in midlatitude weather and climate, and are particularly significant in interpreting aeolian sediments. In this study, we analyzed the behavior and the possible mechanism involved in the change of the westerlies, mainly in terms of the jet stream position, in the mid-Pliocene warm period (3.3 to 3.0 million years ago) using simulations of 15 climate models from the Pliocene Model Intercomparison Project (PlioMIP). Compared to the reference period, the mid-Pliocene midlatitude westerlies generally shifted poleward (approximately 3.6° of latitude in the Northern Hemisphere and 1.9° of latitude in the Southern Hemisphere at 850 hPa level) with a dipole pattern. The dipole pattern of the tropospheric zonal wind anomalies was closely related to the change of the tropospheric meridional temperature gradient as a result of thermal structure adjustment. The poleward shift of the midlatitude westerly jet corresponded to the poleward shift of the mean meridional circulation. The sea surface temperatures and sea ice may have affected the simulated temperature structure and zonal winds, causing the spread of the westerly anomalies in the mid-Pliocene between the atmosphere-only and coupled atmosphere–ocean general circulation model simulations.

Key words: mid-Pliocene, westerly, climate model, PlioMIP

Citation: Li, X. Y., D. B. Jiang, Z. S. Zhang, R. Zhang, Z. P. Tian, and Q. Yan, 2015: Mid-Pliocene westerlies from PlioMIP simulations. *Adv. Atmos. Sci.*, **32**(7), 909–923, doi: 10.1007/s00376-014-4171-7.

1. Introduction

The prevailing westerly winds in the midlatitudes are one of the prominent features of the global atmospheric circulation. They are associated with the vast transport and exchange of heat, moisture and momentum between high and lower latitudes. They play an important role in the weather and climate in the midlatitudes, where the activity of storms along the jet stream influences the variation of heavy precipitation and severe weather (Chang et al., 2002; Yin, 2005; Bengtsson et al., 2006; Rojas, 2013). The movement of jet streams and storm tracks in the westerlies modulates the precipitation patterns in the midlatitudes and, accordingly, the conditions of natural ecosystems, agriculture, and water resources (Seidel et al., 2008). As a fundamental component of the global climate system, the westerlies have an important effect on ocean circulation and the global carbon cycle (Toggweiler et al., 2006; Kuhlbrodt et al., 2007; Toggweiler, 2009). In addition, the position and intensity of westerly winds has been directly related to the aeolian sediments on the Chinese Loess Plateau and in the Pacific Ocean (e.g., Duce et al., 1980; Rea and Leinen, 1988; Rea, 1994; An et al., 2001; Sun, 2004; Sun et al., 2008; Maher, 2011).

Given their critical importance, the westerlies have been a major research focus for decades. The shift of the Southern Hemisphere (SH) westerlies toward the pole, seen in many model simulations, is a response to global warming due to the increasing concentration of atmospheric greenhouse gases (Kushner et al., 2001; Yin, 2005; Ihara and Kushnir, 2009; Wilcox et al., 2012; Chavaillaz et al., 2013; Rojas, 2013). A similar poleward shift of the SH and Northern Hemisphere (NH) westerlies has also been confirmed in recent decades with increasing anthropogenic CO_2 emissions into the atmosphere (Archer and Caldeira, 2008; Pena-Ortiz et al., 2013). This has occurred in tandem with a widening of the tropical belt and an expansion of the Hadley cell (Hu and Fu, 2007; Lu et al., 2007; Seidel et al., 2008; Johanson and Fu, 2009). The opposite effect might be expected in simulations of the last glacial maximum, approximately 21 000 years ago. Specifi-

* Corresponding author: JIANG Dabang
Email: jiangdb@mail.iap.ac.cn

cally, as compared with the pre-industrial reference state, we should perhaps see westerlies shifting equatorward in a cooling climate with a reduction of greenhouse gases. However, while some simulations have shown an equatorward shift, others have shown a poleward shift, or no significant shift at all (Rojas et al., 2009; Chavaillaz et al., 2013; Sime et al., 2013). Thus, there remains an obvious gap in our knowledge with respect to the nature of the midlatitude westerlies. Such limitation casts a shadow over predictions and projections of the westerlies. Examining the characteristics of the westerlies during past warm climate periods, such as the mid-Pliocene, provides us with a potential guide to understanding the behavior of, and mechanisms involved in, the westerlies in a changing climate.

The mid-Pliocene warm period, which occurred approximately 3.3 to 3.0 million years ago, was an interval of relatively warm and stable climate in the Earth's history (Dowsett et al., 2010; Haywood et al., 2010). During this period, the global mean temperature is estimated to have increased by 1.86°C–3.60°C compared with pre-industrial values (Haywood et al., 2013), similar to the climate conditions predicted for the end of the 21st century (Dowsett et al., 2010; Haywood et al., 2010, 2013). Comprehensive and internally consistent paleoenvironmental conditions of the mid-Pliocene have been reconstructed using multiple proxies (e.g., Thompson and Fleming, 1996; Salzmann et al., 2008; Dowsett et al., 2010). Earlier studies of the mid-Pliocene NH westerlies were based only on geological evidence, and the reconstructed climate records of some sediment profiles were used to interpret as the variation of the westerlies. Specifically, the grain size of fine aeolian dust in sediments on the Chinese Loess Plateau and in the North Pacific Ocean was taken as an indicator of the transport power of the westerly winds (e.g., Rea, 1994; Sun et al., 2008). Some proxies of chemical weathering intensity, such as the Rb/Sr ratio (concentration ratio of element Rubidium to Strontium) of lacustrine deposits in the Tarim Basin, have been used to characterize the evolution of westerly winds, in which it was assumed that the Rb/Sr ratio is controlled by precipitation determined by westerly winds (Chang et al., 2013). However, the spatial distribution of proxy data is rather sparse, and is thus likely to record regional signals. Caution should be applied when interpreting regional westerly variation as a continental or global phenomenon. On the other hand, the inherent unreliability and multi-interpretation of proxy data dampen their effectiveness in westerlies-related research. For example, the Rb/Sr ratio is a combination of chemical weathering intensity in the source region and depositional area. The proxy of chemical weather intensity is more closely related to precipitation and temperature, rather than westerly winds.

Numerical experiments have emerged as an efficient way to understand past climates on regional and global scales, and much attention has been given to the mid-Pliocene warm period (e.g., Chandler et al., 1994; Sloan et al., 1996; Jiang et al., 2005; Lunt et al., 2010; Yan et al., 2011; Jiang, 2013; Zhang and Jiang, 2014). With the boundary conditions and reconstructions provided by the U. S. Geological Survey's Pliocene Research Interpretation and Synoptic Mapping (PRISM) project (e.g., Salzmann et al., 2008; Dowsett et al., 2009, 2010), two types of experiments (Table 1), including experiment 1 using atmospheric general circulation models (AGCMs) and experiment 2 using coupled atmosphere–ocean general circulation models (AOGCMs), have recently been designed to simulate the mid-Pliocene climate under the framework of the Pliocene Model Intercomparison Project (PlioMIP) (Haywood et al., 2010, 2011; and references listed in Table 1). Based on those experiments, the large-scale features of the global climate, regional East Asian monsoon, and the dominant components of the mid-Pliocene warming have been analyzed (Haywood et al., 2013; Zhang et al., 2013; Hill et al., 2014). However, the characteristics of the mid-Pliocene westerlies have yet to be studied. Accordingly, this paper

Table 1. Basic information about the models used in this study.

Model ID	Type	Boundary conditions	Atmospheric resolution	Years used for analysis	Reference
CAM3.1	AGCM	Alternate	T42, L26	30	Yan et al. (2012)
CAM4	AGCM	Alternate	T31, L26	20	Zhang and Yan (2012)
ECHAM5	AGCM	Preferred	T31, L19	30	Stepanek and Lohmann (2012)
HadAM3	AGCM	Preferred	$2.5^\circ \times 3.75^\circ$ (lon×lat), L19	30	Bragg et al. (2012)
LMDZ5A	AGCM	Alternate	$\sim 1.9^\circ \times 3.75^\circ$(lon×lat), L39	30	Contoux et al. (2012)
MIROC4m-AGCM	AGCM	Preferred	T42, L20	30	Chan et al. (2011)
MRI-CGCM2.3-AGCM	AGCM	Alternate	T42, L30	50	Kamae and Ueda (2012)
CCSM4	AOGCM	Alternate	$\sim 0.9^\circ \times 1.25^\circ$(lon×lat), L26	30	Rosenbloom et al. (2013)
COSMOS	AOGCM	Preferred	T31, L19	30	Stepanek and Lohmann (2012)
GISS-E2-R	AOGCM	Preferred	$2^\circ \times 2.5^\circ$(lon×lat), L40	30	Chandler et al. (2013)
HadCM3	AOGCM	Alternate	$2.5^\circ \times 3.75^\circ$(lon×lat), L19	50	Bragg et al. (2012)
IPSLCM5A	AOGCM	Alternate	$\sim 1.9^\circ \times 3.75^\circ$(lon×lat), L39	30	Contoux et al. (2012)
MIROC4m	AOGCM	Preferred	T42, L20	30	Chan et al. (2011)
MRI-CGCM2.3	AOGCM	Alternate	T42, L30	50	Kamae and Ueda (2012)
NorESM-L	AOGCM	Alternate	T31, L26	200	Zhang et al. (2012)

presents an analysis of the mid-Pliocene westerlies, mainly through the jet position, from the perspective of multiple climate models, and with an emphasis on the possible dynamic mechanisms involved in the most common changes.

2. Models and methods

2.1. *Boundary conditions and experimental design*

The experiments of 15 models archived in PlioMIP were analyzed, with seven AGCM simulations performed for experiment 1 and eight AOGCMs performed for experiment 2. Each model was used to conduct both a pre-industrial and a mid-Pliocene simulation. The main modification of the mid-Pliocene boundary conditions included changes of the land–sea mask, topography, ice sheet, vegetation, and an increased concentration of atmospheric CO_2 to 405 ppm for both experiments 1 and 2, as well as specified sea surface temperatures (SSTs) and sea ice extent for experiment 1 (Haywood et al., 2010, 2011). The PlioMIP provided a preferred boundary condition data package for all the models able to change the land–sea mask, and also an alternated one to help guide the implementation of the mid-Pliocene topography and vegetation for models with difficulty in land–sea mask modification, to maximize the potential participating groups in PlioMIP (Haywood et al., 2010, 2011). Further details of the model description, boundary condition implementation, experimental design, and the basic climatology of each model simulation can be found in the references listed in Table 1.

2.2. *Model evaluation*

To assess the simulation ability of each model, we evaluated the surface air temperature and zonal and meridional winds on the global scale using the pre-industrial experiments of individual models, in comparison to NCEP–DOE (National Centers for Environmental Prediction–Department of Energy) monthly reanalysis wind data (Kanamitsu et al., 2002) and ERA-Interim monthly reanalysis temperature data (Dee et al., 2011) during 1979–2008. To detect the characteristics of the westerlies and their changes at fine resolution, all model and reanalysis data were aggregated to a horizontal resolution of 0.5° latitude by 0.5° longitude using bilinear interpolation. The model evaluation results are presented using a Taylor diagram (Taylor, 2001), including the spatial correlation coefficient (SCC) and centered root-mean-square error (RMSE) between each pre-industrial simulation and observation (Fig. 1). All 15 models generally performed well in simulating the geographical distribution of climatic elements. Comparatively, the models showed the best skill in simulating temperature, with the values of SCCs larger than 0.99 and

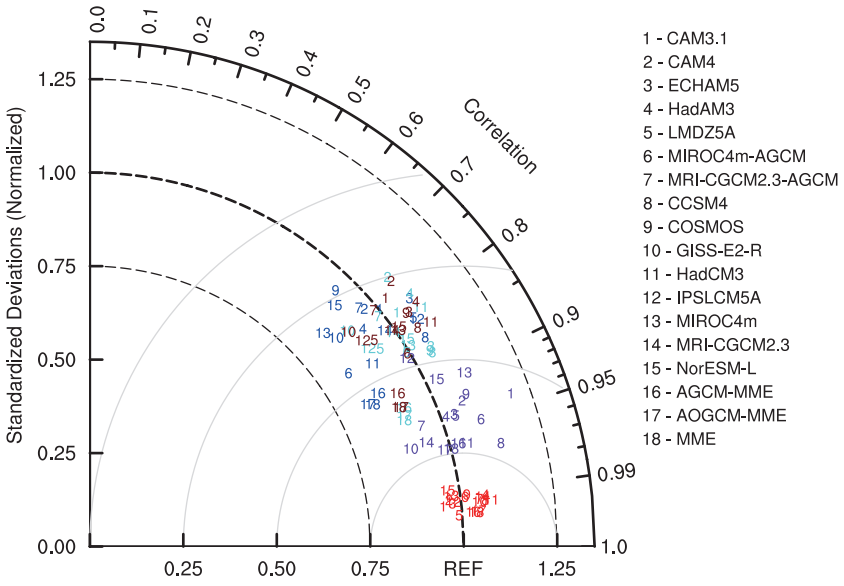

Fig. 1. Taylor diagram (Taylor, 2001) for displaying normalized pattern statistics for zonal and meridional winds at 850 hPa and annual temperature on the global scale between each pre-industrial experiment of the 15 climate models and observation. Each number represents a Model ID: red denotes annual mean temperature; purple and reddish brown denote the annual mean zonal and meridional winds, respectively; and dark and light blue represent the winter and summer meridional winds, respectively. The observation is considered as the reference (REF). Both the root-mean-square error (RMSE) and standard deviation are normalized by the observed standard deviation. The normalized standard deviation of a model is represented by the radial distance from the origin; the spatial correlation coefficient between a model and the reference is shown by the azimuthal position of the model; and the normalized RMSE between a model and the reference is represented by their distance apart.

RMSEs ranging from 0.91 (CAM3.1) to 1.04 (HadCM3). All models reliably reproduced the geographical distribution of zonal and meridional winds at 850 hPa with a certain degree of skill, and the SCCs were larger than 0.70. As a whole, the ensemble means with equal weights of the seven AGCMs, eight AOGCMs, and all 15 models (hereafter referred to as AGCM-MME, AOGCM-MME and MME results respectively) outperformed most of the individual models.

2.3. *Characteristics of the westerlies*

To characterize the variation of the westerlies, we focus on the tropospheric zonal winds at the 850 hPa, 500 hPa, and 200 hPa levels. The zonal winds at upper levels characterize the westerly jet well, and the surface westerly winds interact closely with the ocean and are significant in exploring the atmosphere–ocean momentum, heat, and CO_2 exchanges (Toggweiler et al., 2006; Toggweiler, 2009). Whereas, the tropospheric jet shows upward meridional equatorward tilt and the position of the upper-level westerly jet is not consistent with that of the surface westerly winds; a strong upper-level subtropical jet can hide the changes in near-surface winds. The 850 hPa zonal winds can also characterize the jet and its fluctuations (Chavaillaz et al., 2013; Rojas, 2013; Sime et al., 2013), and wind changes at this level are similar to those at the near surface.

To characterize the shift in position of the westerly jet, the latitudes of both the maximum wind and three specific wind values towards the equator were calculated. A quadratic interpolation around the grid point with maximum mean zonal wind was used to generate the exact maximum wind latitude, as in Chavaillaz et al. (2013). Furthermore, a cubic interpolation around the four grid points with wind speeds close to the specific values was conducted to produce the latitudes of the specific winds. The shift of the westerlies is represented by the latitudinal change of the jet positions between the mid-Pliocene and pre-industrial results.

3. Results

3.1. *Changes of mean zonal winds*

Figure 2 shows the mean zonal winds at 850 hPa from the individual models and their ensemble means. Compared to the reanalysis data, the position of the SH westerly jets simulated by most models (except CCSM4 and HadCM3) tended to migrate far towards the equator, similar to the pre-industrial simulations of the SH westerlies in the work of Rojas (2013).

The features of the westerlies could be extracted from the structures of the mean zonal winds (Fig. 2) and the shift of the westerlies (Fig. 3). In general, the shift directions of the westerlies were consistent between calculations based on the maximum wind and certain specific wind values, and were also similar between calculations in the three levels. However, the results showed that the shift magnitudes calculated by the latitudes of maximum wind were sometimes larger than when calculated by the latitudes of certain wind values, especially at 200 hPa. This result was partly due to the fact that we calculated the latitude of the maximum wind in the whole SH or NH, revealing that the latitude of maximum wind was grid-dependent to some degree.

Relative to the pre-industrial period, all seven sets of AGCM simulations showed a poleward shift of the SH and NH westerlies in the mid-Pliocene. Among the eight sets of AOGCM simulations, COSMOS and HadCM3 simulated a slightly equatorward shift in the position of the SH westerlies, while the other models generally displayed no obvious shift. Almost all AOGCMs reproduced a poleward shift of the NH westerlies, though COSMOS showed an equatorward shift based on latitude changes of some specific wind values.

The multi-model ensemble means all indicated a poleward shift of the NH westerlies, with a magnitude of approximately 3.2° latitude by AGCM-MME, 1.4° latitude by AOGCM-MME, and 3.6° latitude by MME based on the latitudes of the maximum wind at 850 hPa. The AGCM-MME and MME showed a poleward shift of the SH westerlies by 2.6° and 1.9° of latitude based on the latitudes of the maximum wind at 850 hPa, respectively, while the AOGCM-MME showed almost no detectable shift except a slight equatorward shift at 200 hPa. Although the westerly shift in the mid-Pliocene showed a certain inter-model scatter, the poleward shift of the SH/NH westerlies was consistently accompanied by a meridional dipole pattern of the westerly wind change; that is, stronger winds on the poleward flank of the westerly jet and weaker ones on the equatorward flank.

3.2. *Spatial change of the westerlies*

Figure 4 depicts the spatial distribution and change of the mid-Pliocene westerlies compared to the pre-industrial period at 850 hPa. Due to the influence of tall terrain and non-uniform underlying topography, the position of the westerly jet maximum at 850 hPa in the NH continents was scattered greatly along the meridional direction and are hence not shown.

The climatologies of the westerlies at 850 hPa in the pre-industrial and mid-Pliocene simulations (Figs. 4a and 4b) show that strong westerly winds generally distributed with zonal symmetry over the southern oceans, North Pacific, and North Atlantic. The position of the westerly jet stream maximum covered the regions of 45°–50°S over the Southern Ocean and 40°–50°N over the North Pacific and North Atlantic. The position of the mid-Pliocene westerly jet stream maximum tended to shift poleward, with weakening winds along the equatorward flank of the pre-industrial westerly jet, and strengthening ones along the poleward flank (Fig. 4c). The AGCM-MME and AOGCM-MME showed a similar poleward shift of the North Pacific and North Atlantic jets in the mid-Pliocene (Figs. 4d and 4e), although there was an inter-model scatter in the Southern Ocean jet changes. That is, the former showed a clear poleward shift with a dipole structure, and the latter an equatorward shift over the western Southern Pacific but nearly no discernible shift over the other parts of the Southern Ocean. Hence, the spatial distribution of the mid-Pliocene westerly wind anomalies also displayed

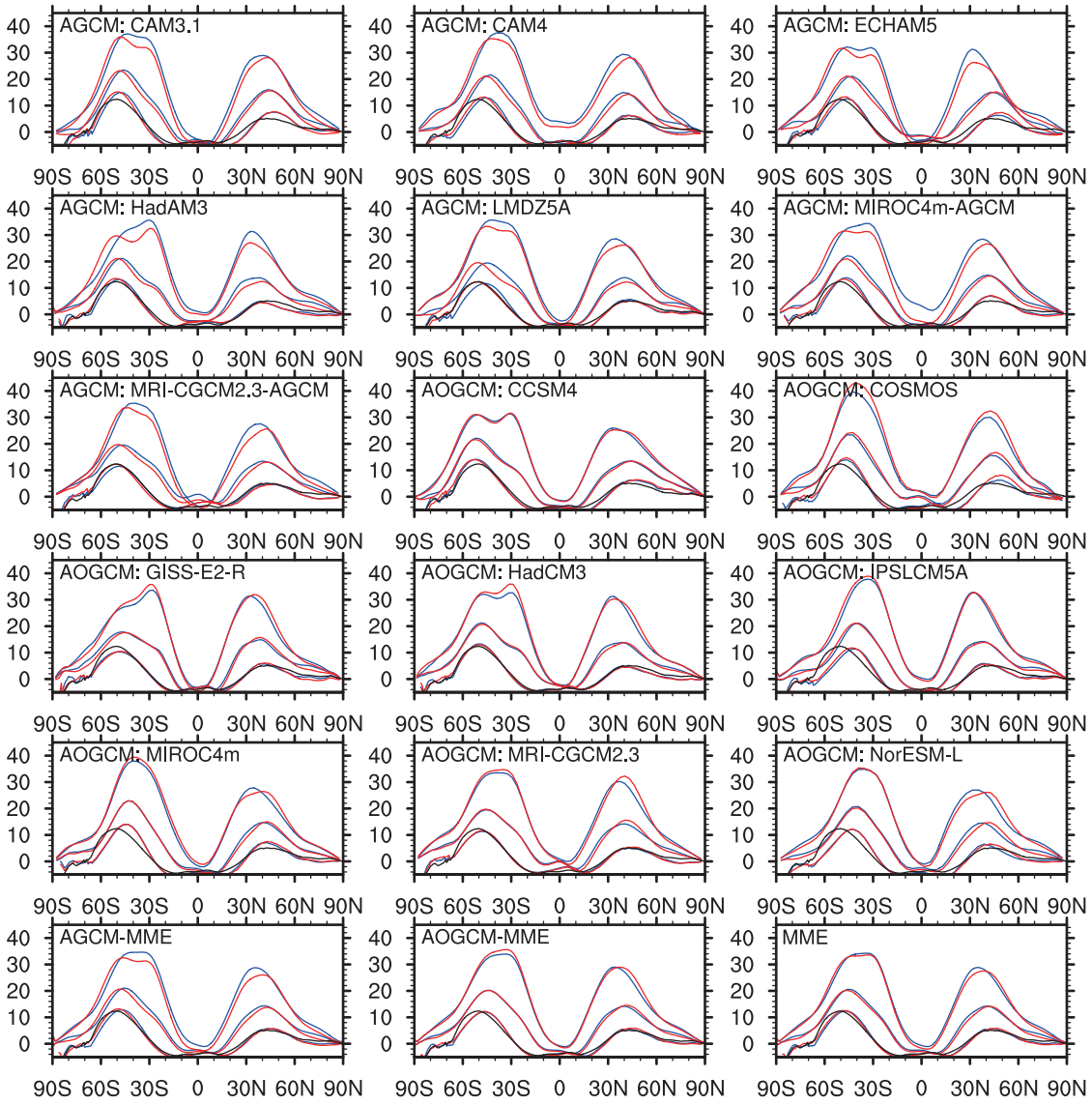

Fig. 2. Climatology of zonal-mean zonal winds (m s^{-1}) for NCEP–DOE reanalysis data (black) and pre-industrial (blue) and mid-Pliocene (red) experiments of the AGCMs and AOGCMs at 850 hPa, 500 hPa, and 200 hPa (the top, middle, and bottom lines in each plot). The AGCM-MME, AOGCM-MME and MME denote the ensemble means of seven AGCMs, eight AOGCMs, and all 15 models, respectively.

a dipole structure, consistent with the features of mean zonal winds (Fig. 2).

Figure 5 shows the difference in zonal winds at 500 hPa and 200 hPa between the mid-Pliocene and pre-industrial period. Five of the six sets of simulations indicated a poleward shift of the position of the mid-Pliocene westerly jet stream maximum, with a dipole pattern on the global scale, similar to that at 850 hPa (Fig. 4). The exception was the AOGCM-MME for the SH westerlies, in which upper-tropospheric westerlies intensified in most areas (Fig. 5f). Inter-model disagreement in the Southern Ocean jet changes between AGCM-MME and AOGCM-MME also existed, with the former indicating a clear poleward shift with a dipole structure that was not apparent in the latter. Meanwhile, westerly jets demonstrated regional characteristics in the vertical direction (Figs. 4 and 5). The dipole pattern of the North Pacific westerly jet was significant and consistent among simulations. As for the Atlantic westerly jet, a dipole pattern occurred mostly in the lower levels (Fig. 4), and it nearly disappeared in the mid and upper levels in the AGCM-MME and AOGCM-MME (Fig. 5). Overall, the changes of the westerlies in the mid and upper levels were comparable to those at lower levels.

4. Discussion

Based on the above analysis, the following two questions need to be answered. What is the possible mechanism underpinning the change of the mid-Pliocene westerly jet, and what gives rise to the dipole structure of the mid-Pliocene anoma-

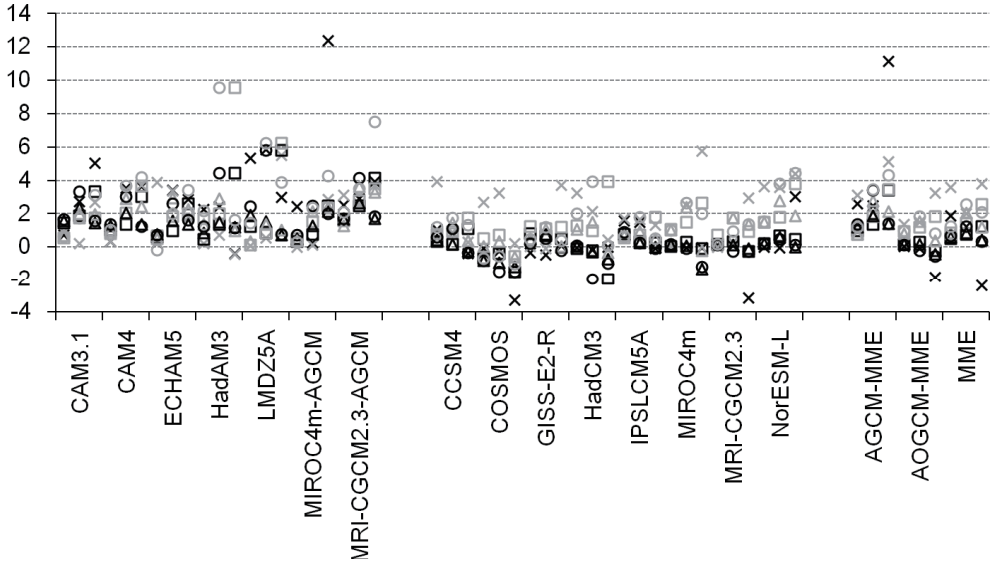

Fig. 3. The poleward shift (units: ° of latitude) of the NH (in gray) and SH (in black) westerly jet in the mid-Pliocene compared to the pre-industrial period. Positive (negative) values mean poleward (equatorward) shift. The three columns in each model are results at 850 hPa, 500 hPa, and 200 hPa. The shift magnitudes are calculated by the latitude changes of the maximum wind (crosses) and of three specific wind values towards the equator (squares, triangles, and circles). The specific wind values (squares, triangles, and circles) are 0, 2, and 4 m s^{-1} at 850 hPa; 4, 8, and 12 m s^{-1} at 500 hPa; and 12, 18, and 24 m s^{-1} at 200 hPa.

lies? In addition, it is equally important to elucidate why the models behave differently.

4.1. *Meridional temperature gradient and westerly winds*

Previous studies have suggested that there is a close relationship between the anomalies of the meridional temperature gradient (MTG) and westerly winds (Lorenz and DeWeaver, 2007; Ihara and Kushnir, 2009; Rojas et al., 2009; Wilcox et al., 2012). From the 15 model simulations, we chose three sets of model results (CAM3.1, CAM4, and NorESM-L) with vertical layer temperature field data available to examine the relationship between the MTG and westerly wind changes.

Figure 6 shows the latitude versus height annual mean temperature, MTG and zonal mean wind differences between the mid-Pliocene and pre-industrial simulations of the aforementioned three models. Compared with the pre-industrial simulation, CAM3.1 and CAM4 generally showed an increasing magnitude of warming from the equator to the pole, and consequently reduced lower- to upper-tropospheric MTGs with reduced zonal winds in the 10° to 40° latitude belt in both hemispheres in the mid-Pliocene. Different conditions occurred in the SH of NorESM-L, which showed increased MTGs and zonal winds in the upper troposphere and the lower stratosphere, although these decreased slightly in the lower troposphere. As for the higher latitudes, both CAM3.1 and CAM4 simulated increased mid- to upper-tropospheric MTGs with strengthening zonal winds between 45°S and 60°S, and both CAM4 and NorESM-L displayed increased tropospheric MTGs and zonal winds between 40°N and 55°N.

According to the thermal wind balance, there is a close relationship between the shear of geostrophic winds and the horizontal temperature gradient. In other words, an increase (a reduction) in MTG would be in accordance with an increase (a decrease) in wind velocity with height. As it is, a meridional dipole pattern of zonal wind change, i.e. positive (negative) wind anomalies in the troposphere centered slightly poleward (equatorward) of the climatological jet (Figs. 6g–i), was generally accompanied by positive (negative) gradient anomalies on the poleward (equatorward) side of the jet (Figs. 6d–f).

The relationship between the zonal winds and MTG changes was significant in the upper troposphere, but not in the lower troposphere (such as the MTG and zonal wind changes between the surface and 850 hPa in the SH in CAM3.1 and CAM4, in Figs. 6d, e, g, and h). This was partly due to the direction of the upper-tropospheric winds, which were more consistent with the thermal winds. Such variation followed increased MTG along the upper troposphere in the midlatitudes. The lower-tropospheric zonal wind anomalies were roughly in-phase with those in the mid-levels, when the meridional dipole patterns of tropospheric zonal wind and MTG anomalies were significant. Thus, in the mid-Pliocene compared with the pre-industrial period, from the perspective of the thermal wind equation, both the lower- and upper-level zonal wind anomalies were related overall to the mid- and upper-level MTG anomalies as a result of atmospheric thermal structure adjustment.

4.2. *Mean meridional circulation and westerly winds*

The mean meridional circulation (MMC) was closely related to the poleward shift of the westerly jet in the mid-

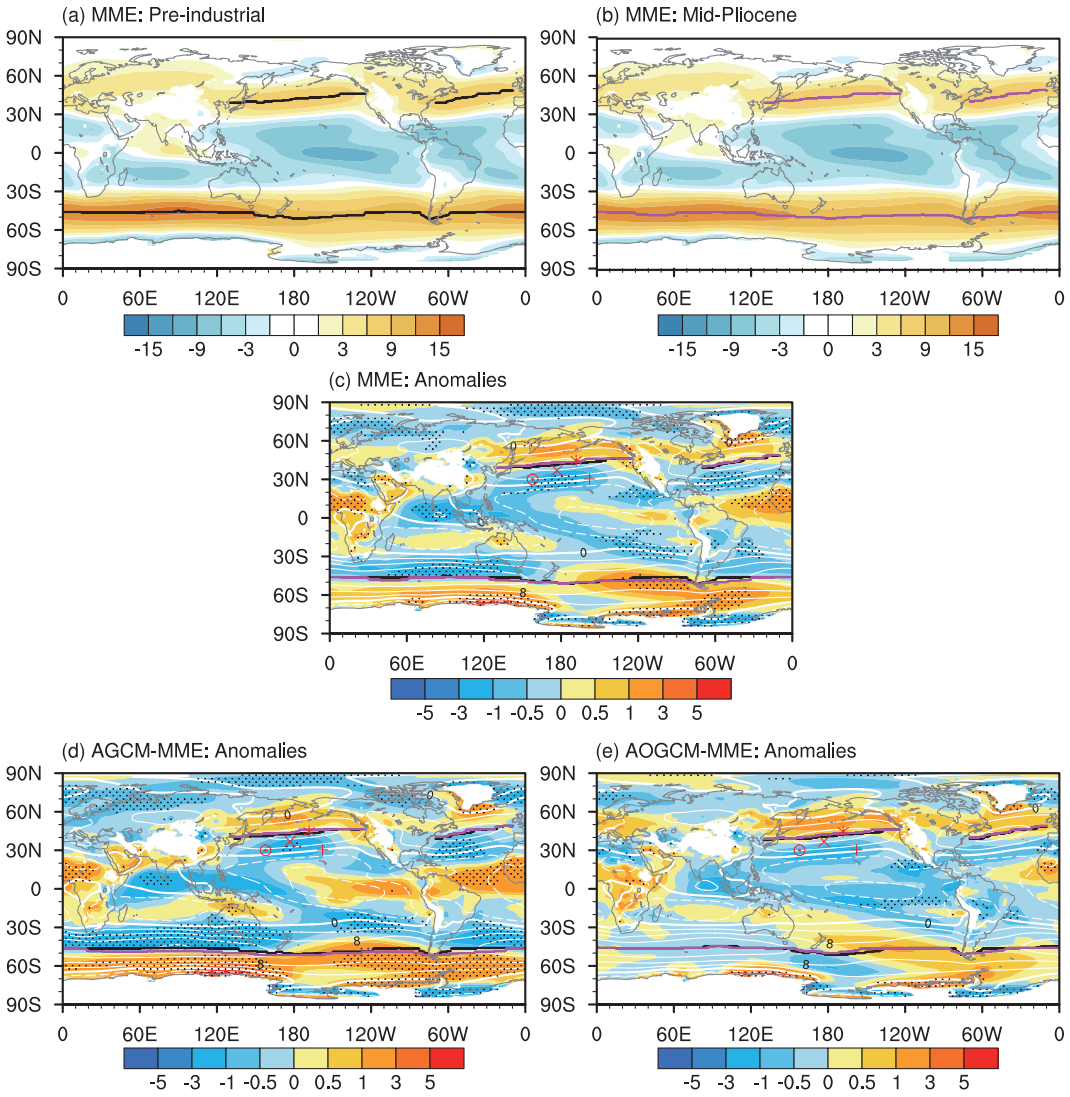

Fig. 4. Climatology of annual mean zonal winds at 850 hPa for the MME: (a) pre-industrial, (b) mid-Pliocene, (c) anomalies (mid-Pliocene minus pre-industrial), and for the anomalies in (d) AGCM-MME and (e) AOGCM-MME. The colored bars represent the wind speed (m s^{-1}). The white contours (c, d and e) represent the zonal wind speed (solid, westerly winds; dashed, easterly winds; scaled by 4 m s^{-1}) in the pre-industrial period. The black and magenta lines represent the position of the pre-industrial and mid-Pliocene jet stream maximum, represented by latitudes of meridional maximum zonal winds of each hemisphere in the pre-industrial and mid-Pliocene periods. The areas with confidence levels larger than 90% are dotted. The markers in (c–e) represent the positions of Deep Sea Drilling Project sites 305 (circle), 310 (cross), and GPC3 (plus sign), as well as the Ocean Deep-Sea Project site 885/886 (asterisk), which provide the paleoenvironment evidence discussed in section 4.4.

Pliocene. In this study, the zonal mean MMC was calculated by a meridional mass stream function, as illustrated in Figs. 6j–l. All models simulated a less intense and poleward-extended Hadley cell, except in the SH in NorESM-L, and a poleward shift of the Ferrel cell, except in the NH in CAM3.1 and the SH in NorESM-L. In the SH, CAM3.1 and CAM4 simulated a poleward shift of the MMC (weakened southern Hadley cell and strengthened poleward flank of the Ferrel cell), coherent with a poleward shift of the mid-latitude jet, while NorESM-L simulated a slightly equatorward shift of the MMC (strengthened equatorward flank and weakened poleward flank of the southern Hadley cell, and a slightly contracted Ferrel cell), accompanied by no significant shift of the midlatitude jet. In addition, in the NH, CAM4 and NorESM-L simulated a poleward shift of the MMC (weakened northern Hadley cell, and a poleward-shifted Ferrel cell), accompanied by a poleward shift of the midlatitude jet. Thus, the shift of the midlatitude jet should correspond to the change of the MMC.

The Hadley cell has also been found to generally weaken in other mid-Pliocene model simulations (Jiang et al., 2005; Kamae et al., 2011; Sun et al., 2013). In the mid-Pliocene period, the ascending Hadley cell weakened and expanded poleward in MRI-CGCM2.3 AGCM simulations (Kamae et

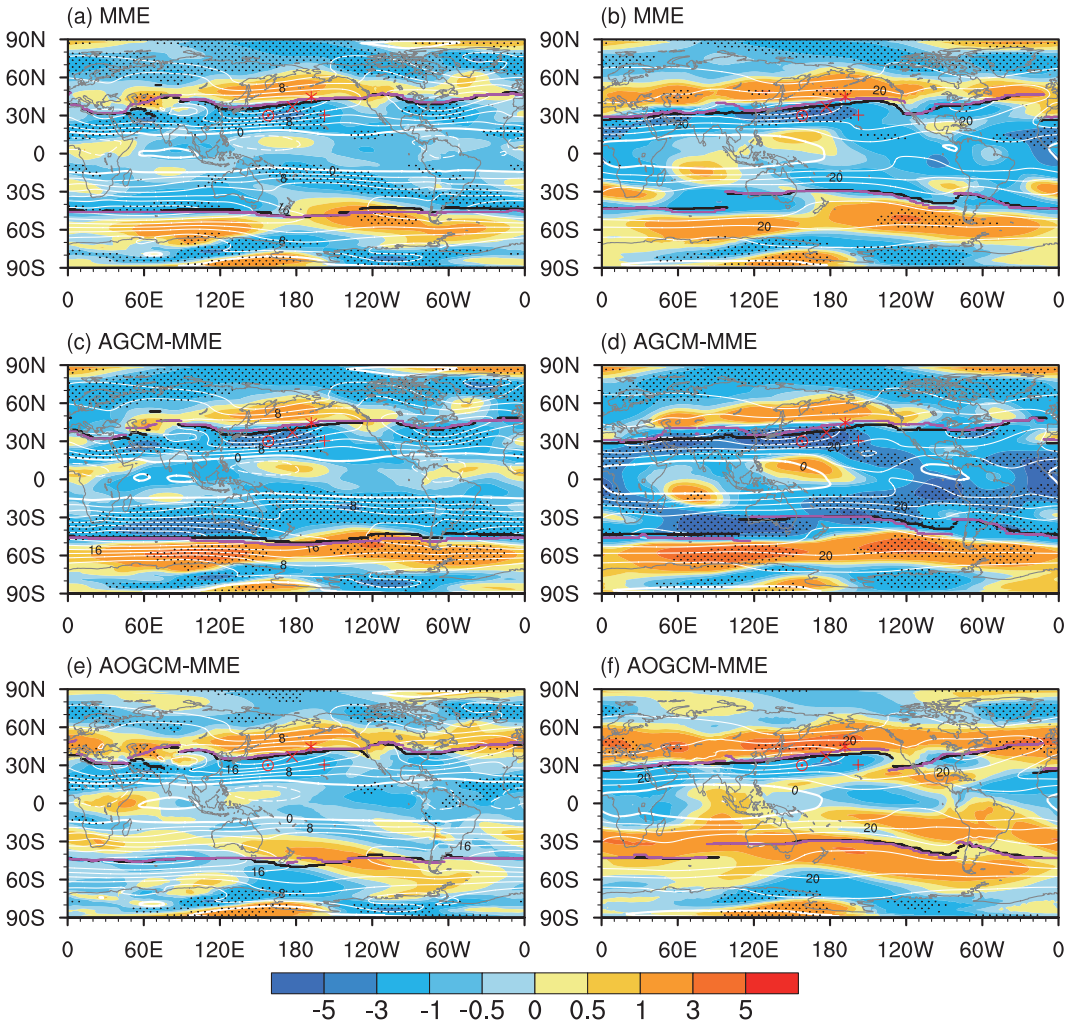

Fig. 5. The same as in Figs. 4c–e, but for (a, c, e) 500 hPa and (b, d, f) 200 hPa.

al., 2011); And in IPSLCM5A, the Hadley cell expanded poleward, with a decreased northern tropical Hadley cell intensity and an intensified subtropical Hadley cell (Sun et al., 2013). Compared to the IPSLCM5A simulations, the present NorESM-L results also showed a weakened and poleward-expanded northern Hadley cell and strengthened southern Hadley cell. By contrast, the IPSLCM5A results indicated a slight poleward shift of the southern Hadley cell, while the NorESM-L results displayed nearly no shift.

Furthermore, the poleward shift of the Ferrel cell was always accompanied by a poleward shift of the midlatitude jet (Figs. 6g–i and 6d–f). Thus, it seems that the change of the polar boundary of the Ferrel cell was more closely associated with the shift of the midlatitude jet. Perhaps the poleward shifting of the Ferrel cell corresponded to the eddy activity that extended poleward, as implied by the increasing MTGs in the polar flank of the Ferrel cell (Figs. 6d–f).

4.3. *Inter-model comparison*

Based on the availability of wind data in the vertical layers, we chose 11 (five AGCMs and six AOGCMs) out of 15 sets of simulations to explore the possible reasons for the inter-model scatter of the midlatitude westerly jet change (Fig. 7). Generally, the AGCMs showed good agreement in terms of the mid-Pliocene poleward shift of the SH westerly jets, although the magnitude of the wind velocity anomalies had a certain degree of inter-model spread. For the AOGCMs, the poleward shift with a dipole pattern was significant in the NH westerly jet in all simulations, and in the SH westerly jet in CCSM4 only. The upward expansion of the SH westerly jet with strengthened winds in the upper troposphere, and the slightly decreased or little changed winds in the lower troposphere, were simulated by the remaining five AOGCMs. There was no discernible meridional shift of the SH westerly jets. Taking all models into account (Fig. 7), the poleward shift of the westerly jet with the dipole pattern was presented in the AGCM-MME and MME, while AOGCM-MME showed no discernible meridional shift of the SH westerly jet. In other words, the poleward shift of the SH (NH) westerly jet with the dipole pattern was more significant in the AGCMs (AOGCMs) (Fig. 7).

The mid-Pliocene zonal wind changes should correspond to the MTG anomalies through atmospheric thermal structure adjustment. The difference of the mid-Pliocene wester-

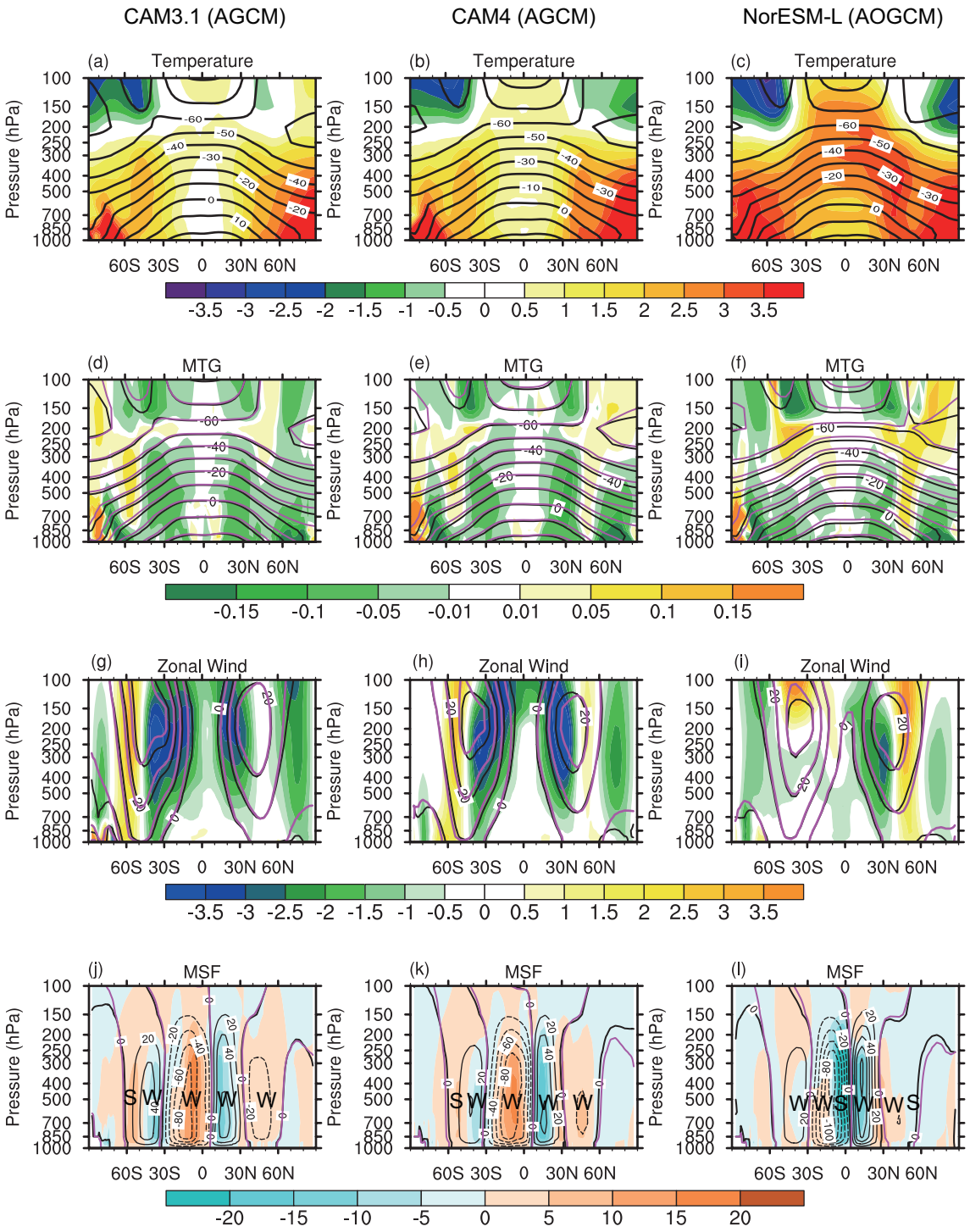

Fig. 6. Anomalies (mid-Pliocene minus pre-industrial) of zonal mean temperature (a–c, °C), meridional temperature gradient (MTG, d–f, K deg^{-1}), zonal winds (g–i, m s^{-1}), and mass stream function (MSF, j–l, $\times 10^9$ kg s^{-1}) from CAM3.1 (left), CAM4 (central), and NorESM-L (right), respectively. Black (magenta) contours (a–f) denote the pre-industrial (mid-Pliocene) temperature (scaled by 10°C), and black (magenta) contours (g–i) denote the pre-industrial (mid-Pliocene) zonal mean winds (scaled by 10 m s^{-1}). In plots of MSF (j–l), black contours indicate the pre-industrial MSF ($\times 10^9$ kg s^{-1}), magenta contours denote the zero contour of the mid-Pliocene MSF ($\times 10^9$ kg s^{-1}), positive (negative) contours indicate clockwise (counterclockwise) circulation, W and S mean weakened and strengthened MSF, and the shading denotes anomalies. The meridional temperature gradient is defined as the difference per latitude between the temperatures of two grids (the northern one minus the nearby southern one). Note that for easier interpretation, absolute values of temperature gradients were calculated in each hemisphere, as in Rojas (2013).

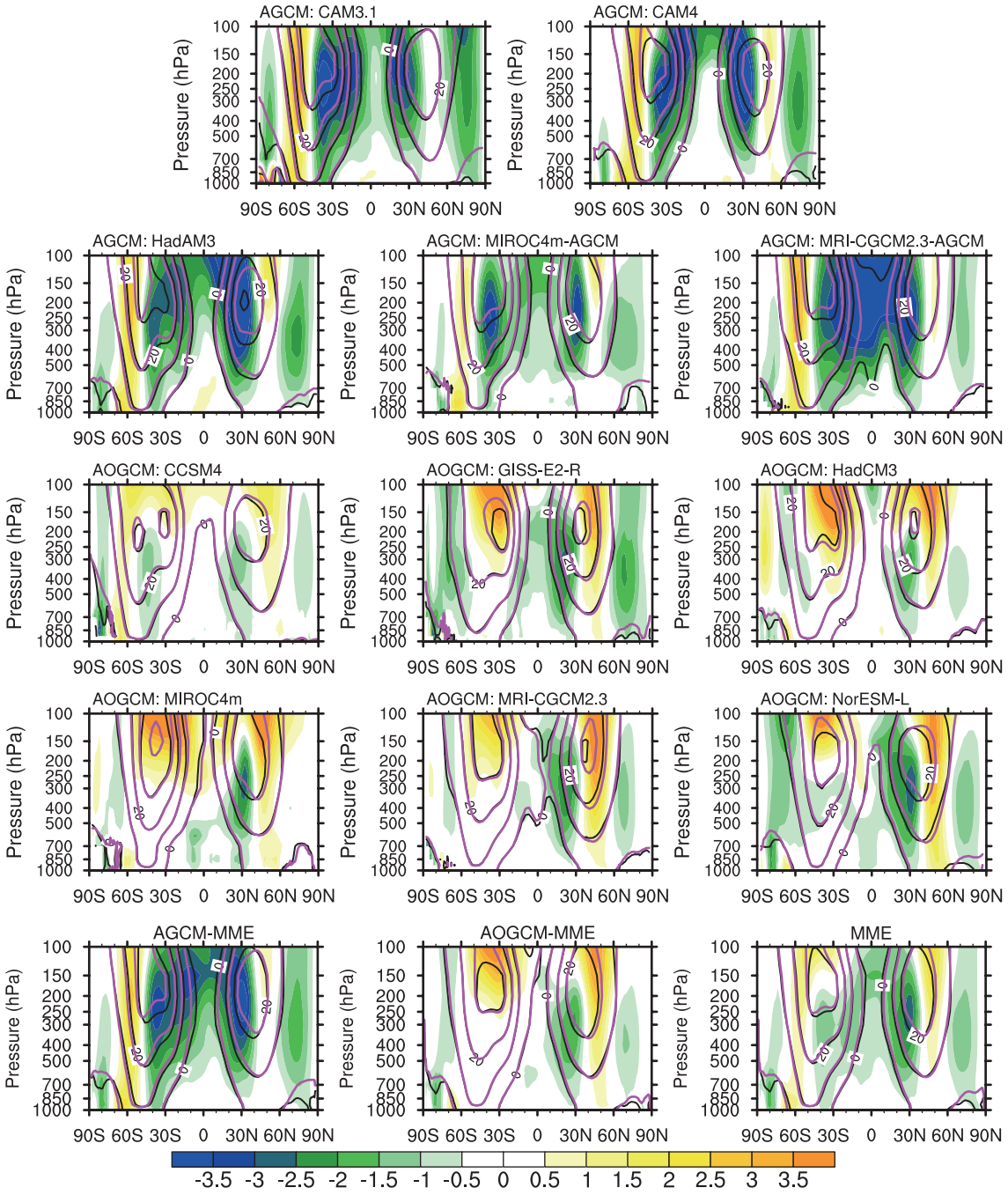

Fig. 7. Anomalies (mid-Pliocene minus pre-industrial) of mean zonal winds in AGCMs and AOGCMs. The black and magenta contours are pre-industrial and mid-Pliocene mean zonal winds (scaled by 10 m s^{-1}), respectively. Shaded areas show the anomalies (m s^{-1}).

lies between the AGCMs and AOGCMs (Fig. 7) means that the thermal structure adjustment behaves differently. Due to the more prominent dipole pattern and intensified NH poleward flank westerly winds in the AOGCMs, larger MTGs in the northern midlatitudes in the AOGCMs were expected, as shown by NorESM-L based on the thermal wind balance (Fig. 6c). Such an expectation seems correct, because the AOGCM-MME simulated warmer tropical and weaker northern high latitude temperature anomalies relative to the AGCM-MME (Haywood et al., 2013). This contributed to steeper MTGs in the northern midlatitudes in the AOGCM-MME, and hence more remarkably strengthened zonal winds at the polar flank of the NH westerly jet (Fig. 7).

The variation of SST and sea ice extent were the main factors determining the mid-Pliocene climate, if not considering the variation of greenhouse gas concentrations (Jiang et al., 2005), and were among the first order controls on the mid-Pliocene climate change relative to the pre-industrial period (Haywood et al., 2013). Previous research has indicated that the warmer early-Pliocene SST influenced the global air

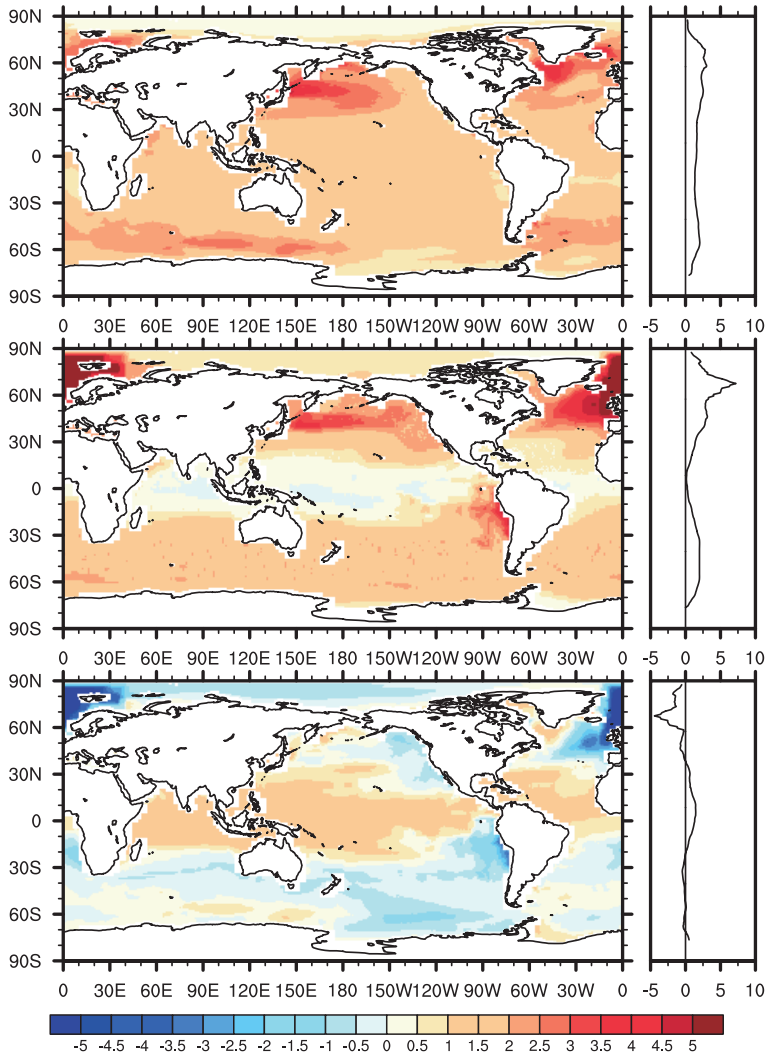

Fig. 8. The mid-Pliocene minus pre-industrial differences in SSTs (left, °C) and their zonal means (right, °C) as dervied from the simulation of AOGCM-MME (top) and the reconstruction used to drive AGCMs (middle). The bottom panel denotes AOGCM-MME minus reconstruction.

temperature by affecting radiation through the impact of increasing water vapor and cloud cover and the consequential reduction of outgoing longwave radiation at the top of the atmosphere (Brierley et al., 2009; Brierley and Fedorov, 2010). In addition, Hill et al. (2014) indicated that, in mid-Pliocene simulations by AOGCMs, sea ice was one of the important components in the energy balance in high latitudes, mainly through its influence on clear-sky albedo. Also, climate sensitivity experiments have demonstrated that the mid-Pliocene Arctic terrestrial surface air temperatures were extremely sensitive to the spatial and seasonal extent of sea ice (Ballantyne et al., 2013).

However, the treatment of SSTs and sea ice differed between the AGCMs and AOGCMs: the SSTs and sea ice were fixed in the former but calculated in the latter. Compared with the specified SSTs from reconstructions established by the PRISM project in the AGCM experiments, the SSTs in the AOGCMs were generally underestimated in the northern mid- and high-latitudes, relative to the reconstructions (Dowsett et al., 2012, 2013; Haywood et al., 2013). As shown in Figure 8, in the AOGCM-MME (AGCM) result, the SST anomaly consisted of moderate (nearly unchanged) warming in the tropics and higher warming in the high-latitudes, and was generally in accordance with the scenario of the surface air temperature anomaly (Figs. 2 and 3 in Haywood et al., 2013). Therefore, the equator-to-pole temperature gradient reduced, and the Hadley Cell weakened. Furthermore, the Hadley cell in the AGCMs weakened to a greater extent, corresponding to the more severely reduced equator-to-pole temperature gradient as a result of less tropical warming in the mid-Pliocene, and in turn the greater decreased tropospheric zonal westerly winds in the low-latitudes (Figs. 6g and 6h). Additionally, compared to the reconstructed sea ice extent, PlioMIP simulations showed that the simulated mid-Pliocene sea ice amount varied from model to model (Fig. 7c in Hill et al., 2014). Due to the different treatments of sea ice, the sea

ice extent and consequently the clear-sky albedo and energy balance in the high-latitudes, would be different between the AGCMs and AOGCMs.

Previous studies have revealed that both radiation-induced effects of atmospheric CO_2 and rising SSTs are important for the poleward shift of the westerlies (and changes in the zonal-mean MMC) (Kodama et al., 2007; Kawatani et al., 2012; Grise and Polvani, 2014). Furthermore, sensitivity experiments on a future warming climate have indicated that the tropospheric warming derives mainly from the SST change, and the stratosphere cooling is due mainly to the increased CO_2 (Kawatani et al., 2012). Considering the CO_2 concentration was the same between the AGCMs and AOGCMs, the fact that the SST patterns between the AOGCMs and AGCMs were different and the tropospheric warmth over the tropics was larger in the former (Fig. 6c) than that in the latter (Figs. 6a–b), testified the important role of the SST in the atmospheric thermal adjustment and corresponding circulation change.

As such, we speculate that the SST and sea ice may have impacted greatly on the simulated temperature structure and zonal winds, resulting in the spread of the westerly anomalies between the AOGCM and AGCM experiments.

4.4. *Model–data comparison*

Reconstructing the history of the westerlies based on limited paleoenvironmental data with uncertainties and/or interpretation ambiguity is complicated. The limited number of convincing paleoclimatic evidence for the NH westerlies in the mid-Pliocene derives mainly from the aeolian sediments on the Chinese Loess Plateau (e.g., Sun, 2004; Sun et al., 2008) and from certain North Pacific deep-sea sites (e.g., Rea and Leinen, 1988; Rea, 1994). However, Qiang et al. (2010) concluded that caution should be exercised when using the fine dust records on the Chinese Loess Plateau as an indicator of the characteristics of the westerlies. It is more robust to use the North Pacific deep-sea aeolian sediments to retrieve the westerly intensity.

The grain size of the pelagic aeolian dust in the North Pacific deep-sea is a function of wind intensity, allowing the estimation of the intensity of the transporting wind (Janecek and Rea, 1985; Rea, 1994; Rea et al., 1998). Far from the source area of inland Asia, the aeolian grain size in the deep-sea has been found to be in equilibrium with the transporting winds, and therefore used as an indicator of their energy (Janecek and Rea, 1985). Larger grains correspond to stronger winds. Figure 9 shows the median aeolian grain size records since the mid-Pliocene from three Deep Sea Drilling Project sites (305, 310 and GPC3) and one Ocean Deep-Sea Project site 885/886. Although the temporal resolution for these four records was relatively large, they showed smaller grain size during the mid-Pliocene than the late Quaternary, indicating that mid-Pliocene westerly winds were relatively weaker.

The smaller aeolian grain size, serving as evidence of weaker westerly winds in the mid-Pliocene, was overall consistent with the weakened mid-Pliocene zonal winds on the equatorward flank of the westerly jet in the simulations (Figs. 4c, 5a, and 5b). Also noted was model–data discrepancy. The weakened westerly winds, suggested by the smaller mid-Pliocene median aeolian grain size from site 885/886 compared to its recent geological epoch, was contrary to the strengthened mid-Pliocene westerly winds in the MME (Figs. 4c, 5a and 5b) and AOGCM-MME (Figs. 4e, 5e and 5f), although it agreed with the weakened mid-Pliocene westerly winds in the AGCM-MME (Figs. 4d, 5c and 5d). Such model–data discrepancy is likely related to the uncertainty in paleoenvironmental data, the deficiencies of climate models, and the uncertainty in reconstructed boundary conditions. Specifically, the mid-Pliocene boundary conditions impacted the simulated atmospheric thermal structure adjustment, and in turn the westerly winds. Previous simulations have revealed that the increased greenhouse gases had a dominant role in tropical warming, and the prescribed ice sheet and vegetation and simulated sea ice and snow albedo feedbacks are of significance in the high-latitudes (Hill et al., 2014). In some regions, such as Greenland, where the elevation decreased by about 1800 m, the mid-Pliocene warmth was mainly due to the topographic effect (Stepanek and Lohmann, 2012). In addition, the specified SSTs and sea ice used to drive the AGCMs impacted greatly on the simulated temperature structure and zonal winds in the troposphere. Therefore, more accurately reconstructed boundary conditions would contribute to a more realistic simulation of the mid-Pliocene

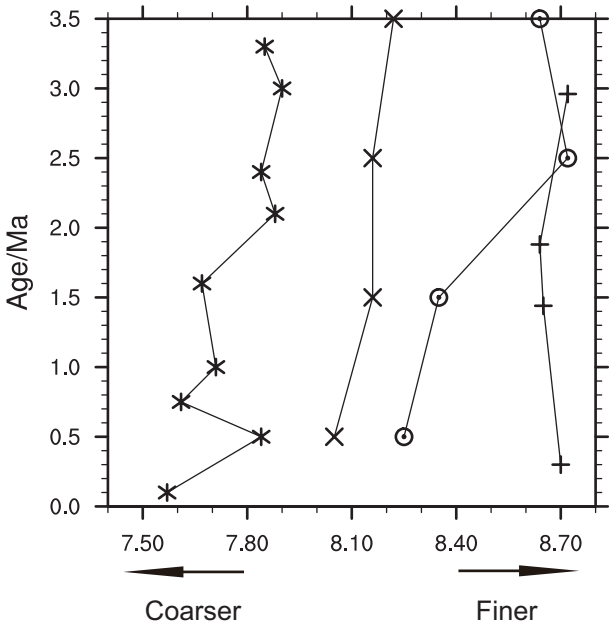

Fig. 9. Median grain size (Φ50) of aeolian dust at deep-sea sites beneath the prevailing westerlies. Phi (Φ) units are a logarithmic size scale, and Φ equals the negative log to the base 2 of the grain diameter in millimeters. The value of Φ gets larger as the grain size gets finer, and a median grain size of 8Φ corresponds to 4 μm diameter grains. The asterisks, crosses, circles with dots, and plus sign markers represent the grain sizes at sites 885/886, 310, 305, and GPC3, respectively. The data were obtained from Rea and Janecek (1982) and Rea et al. (1998).

westerlies.

5. Summary

In this study, we analyzed the change and the possible underlying mechanism of the mid-Pliocene westerlies using the experiments of seven AGCMs and eight AOGCMs in PlioMIP. In general, all models reliably reproduced the climatic elements of concern, and the multi-model mean outperformed most of the individual models. Although there was an inter-model scatter on the mid-Pliocene change in the westerlies, the poleward shift of the westerlies in the SH (approximately 1.9° of latitude at 850 hPa level) and NH (approximately 3.6° of latitude at 850 hPa level) was characteristic and was accompanied by a meridional dipole pattern of the westerly wind change, namely stronger winds on the poleward flank of the midlatitude westerly jet and weaker winds on the equatorward flank.

Due to the atmospheric thermal structure adjustment, the upper-tropospheric MTGs altered accordingly in the midlatitudes, and played an important role in the roughly in-phase variation of the zonal wind anomalies in the troposphere through thermal wind balance, especially when the meridional dipole patterns of tropospheric zonal wind and MTG anomalies were significant. On the other hand, the mid-Pliocene westerly jet's poleward shift with a dipole pattern corresponded to the poleward shift of the mean meridional circulation (both the Hadley and Ferrel cells). The different treatments of SSTs and sea ice between AGCMs and AOGCMs were speculated to impact greatly on the simulated temperature structure and zonal winds, and in turn result in the difference of the westerly anomalies between the experiments of the AOGCMs and AGCMs.

Limited number of convincing geological evidence from North Pacific deep-sea sites supports the major features of the simulated North Pacific westerlies, and confirms the simulated weakening of mid-Pliocene zonal winds on the equatorward flank of the westerly jet, although there was a degree of model–data discrepancy. More reconstruction work using multiple proxies and methods is required to provide convincing paleoenvironmental evidence and narrow the uncertainty of the mid-Pliocene boundary conditions, and more simulations are needed to deepen our understanding of the mid-Pliocene climate.

Acknowledgements. We sincerely thank the anonymous reviewers for their insightful comments. We also acknowledge the Pliocene Model Intercomparison Project (PlioMIP) modeling groups (listed in Table 1 of this paper) for producing and making available their model output. Thanks are due to SUI Yue, HAO Xin, SU Baohuang, LIU Ke, and HU Qin for valuable discussion, and to M. ROJAS for very useful consultations. This work was supported by the Strategic Priority Research Program of the Chinese Academy of Sciences (Grant No. XDB03020602), and the National Natural Science Foundation of China (Grant Nos. 41430962 and 41421004).

REFERENCES

An, Z., J. E. Kutzbach, W. L. Prell, and S. C. Porter, 2001: Evolution of Asian monsoons and phased uplift of the Himalaya-Tibetan plateau since Late Miocene times. *Nature*, **411**, 62–66.

Archer, C. L., and K. Caldeira, 2008: Historical trends in the jet streams. *Geophys. Res. Lett.*, **35**, L08803, doi: 10.1029/2008GL033614.

Ballantyne, A. P., Y. Axford, G. H. Miller, B. L. Otto-Bliesnere, N. Rosenbloome, and J. W. C. White, 2013: The amplification of Arctic terrestrial surface temperatures by reduced sea-ice extent during the Pliocene. *Palaeogeography, Palaeoclimatology, Palaeoecology*, **386**, 59–67.

Bengtsson, L., K. I. Hodges, and E. Roeckner, 2006: Storm tracks and climate change. *J. Climate*, **19**, 3518–3543.

Bragg, F. J., D. J. Lunt, and A. M. Haywood, 2012: Mid-Pliocene climate modelled using the UK Hadley Centre Model: PlioMIP Experiments 1 and 2. *Geoscientific Model Development*, **5**, 1109–1125.

Brierley, C. M., and A. V. Fedorov, 2010: Relative importance of meridional and zonal sea surface temperature gradients for the onset of the ice ages and Pliocene-Pleistocene climate evolution. *Paleoceanography*, **25**, PA2214, doi: 10.1029/2009PA001809.

Brierley, C. M., A. V. Fedorov, Z. Liu, T. D. Herbert, K. T. Lawrence, and J. P. LaRiviere, 2009: Greatly expanded tropical warm pool and weakened Hadley circulation in the early Pliocene. *Science*, **323**, 1714–1718.

Chan, W.-L., A. Abe-Ouchi, and R. Ohgaito, 2011: Simulating the mid-Pliocene climate with the MIROC general circulation model: Experimental design and initial results. *Geoscientific Model Development*, **4**, 1035–1049.

Chandler, M., D. Rind, and R. Thompson, 1994: Joint investigations of the middle Pliocene climate II: GISS GCM northern hemisphere results. *Global and Planetary Change*, **9**, 197–219.

Chandler, M. A., L. E. Sohl, J. A. Jonas, H. J. Dowsett, and M. Kelley, 2013: Simulations of the mid-Pliocene warm period using two versions of the NASA/GISS ModelE2-R coupled Model. *Geoscientific Model Development*, **6**, 517–531.

Chang, E. K. M., S. Lee, and K. L. Swanson, 2002: Storm track dynamics. *J. Climate*, **15**, 2163–2183.

Chang, H., Z. S. An., F. Wu., Z. D. Jin., W. G. Liu., and Y. G. Song, 2013: A Rb/Sr record of the weathering response to environmental changes in westerly winds across the Tarim Basin in the late Miocene to the early Pleistocene. *Palaeogeography, Palaeoclimatology, Palaeoecology*, **386**, 364–373.

Chavaillaz, Y., F. Codron, and M. Kageyama, 2013: Southern westerlies in LGM and future (RCP4.5) climates. *Climate of the Past*, **9**, 517–524.

Contoux, C., G. Ramstein, and A. Jost, 2012: Modelling the mid-Pliocene warm period climate with the IPSL coupled model and its atmospheric component LMDZ5A. *Geoscientific Model Development*, **5**, 903–917.

Dee, D. P., and Coauthors, 2011: The ERA-Interim reanalysis: Configuration and performance of the data assimilation system. *Quart. J. Roy. Meteor. Soc.*, **137**, 553–597.

Dowsett, H. J., M. M. Robinson, and K. M. Foley, 2009: Pliocene three-dimensional global ocean temperature reconstruction. *Climate of the Past*, **5**, 769–783.

Dowsett, H., and Coauthors, 2010: The PRISM3D paleoenviron-

mental reconstruction. *Stratigraphy*, **7**, 123–139.

Dowsett, H. J., and Coauthors, 2012: Assessing confidence in Pliocene sea surface temperatures to evaluate predictive models. *Nature Climate Change*, **2**, 365–371.

Dowsett, H. J., and Coauthors, 2013: Sea surface temperature of the mid-Piacenzian ocean: A data-model comparison. *Scientific Reports*, **3**, doi: 10.1038/srep02013.

Duce, R. A., C. K. Unni, B. J. Ray, J. M. Prospero, and J. T. Merrill, 1980: Long-range atmospheric transport of soil dust from Asia to the tropical North Pacific: Temporal variability. *Science*, **209**, 1522–1524.

Grise, K. M., and L. M. Polvani, 2014: The response of midlatitude jets to increased CO_2: Distinguishing the roles of sea surface temperature and direct radiative forcing. *Geophys. Res. Lett.*, **41**, 6863–6871.

Haywood, A. M., and Coauthors, 2010: Pliocene Model Intercomparison Project (PlioMIP): Experimental design and boundary conditions (experiment 1). *Geoscientific Model Development*, **3**, 227–242.

Haywood, A. M., H. J. Dowsett, M. M. Robinson, D. K. Stoll, A. M. Dolan, D. J. Lunt, B. Otto-Bliesner, and M. A. Chandler, 2011: Pliocene Model Intercomparison Project (PlioMIP): Experimental design and boundary conditions (experiment 2). *Geoscientific Model Development*, **4**, 571–577.

Haywood, A. M., and Coauthors, 2013: Large-scale features of Pliocene climate: Results from the Pliocene Model Intercomparison Project. *Climate of the Past*, **9**, 191–209.

Hill, D. J., and Coauthors, 2014: Evaluating the dominant components of warming in Pliocene climate simulations. *Climate of the Past*, **10**, 79–90.

Hu, Y., and Q. Fu, 2007: Observed poleward expansion of the Hadley circulation since 1979. *Atmos. Chem. Phys.*, **7**, 5229–5236.

Ihara, C., and Y. Kushnir, 2009: Change of mean midlatitude westerlies in 21st century climate simulations. *Geophys. Res. Lett.*, **36**, L13701, doi: 10.1029/2009GL037674.

Janecek, T. R., and D. K. Rea, 1985: Quaternary fluctuations in the northern hemisphere trade winds and westerlies. *Quaternary Research*, **24**, 150–163.

Jiang, D. B., 2013: Vegetation feedback at the mid-Pliocene. *Atmospheric and Oceanic Science Letters*, **6**, 320–323.

Jiang, D. B., H. J. Wang, Z. L. Ding, X. M. Lang, and H. Drange, 2005: Modeling the middle Pliocene climate with a global atmospheric general circulation model. *J. Geophys. Res.*, **110**, D14107, doi: 10.1029/2004JD005639.

Johanson, C. M., and Q. Fu, 2009: Hadley cell widening: Model simulations versus observations. *J. Climate*, **22**, 2713–2725.

Kamae, Y., and H. Ueda, 2012: Mid-Pliocene global climate simulation with MRI-CGCM2.3: Set-up and initial results of PlioMIP Experiments 1 and 2. *Geoscientific Model Development*, **5**, 383–423.

Kamae, Y., H. Ueda, and A. Kitoh, 2011: Hadley and Walker circulations in the mid-Pliocene warm period simulated by an atmospheric general circulation model. *J. Meteor. Soc. Japan*, **89**, 475–493.

Kanamitsu, M., W. Ebisuzaki, J. Woollen, S. Yang, J. J. Hnilo, M. Fiorino, and G. L. Potter, 2002: NCEP–DOE AMIP-II Reanalysis (R-2). *Bull. Amer. Meteor. Soc.*, **83**, 1631–1643.

Kawatani, Y., K. Hamilton, and A. Noda, 2012: The effects of changes in sea surface temperature and CO_2 concentration on the Quasi-Biennial Oscillation. *J. Atmos. Sci.*, **69**, 1734–1749.

Kodama, C., T. Iwasaki, K. Shibata, and S. Yukimoto, 2007: Changes in the stratospheric mean meridional circulation due to increased CO_2: Radiation- and sea surface temperature-induced effects. *J. Geophys. Res.*, **112**, D16103, doi: 10.1029/2006JD008219.

Kuhlbrodt, T., A. Griesel, M. Montoya, A. Levermann, M. Hofmann, and S. Rahmstorf, 2007: On the driving processes of the Atlantic meridional overturning circulation. *Reviews of Geophysics*, **45**, RG2001, doi: 10.1029/2004RG000166.

Kushner, P. J., I. M. Held, and T. L. Delworth, 2001: Southern hemisphere atmospheric circulation response to global warming. *J. Climate*, **14**, 2238–2249.

Lorenz, D. J., and E. T. DeWeaver, 2007: Tropopause height and zonal wind response to global warming in the IPCC scenario integrations. *J. Geophys. Res.*, **112**, D10119, doi: 10.1029/2006JD008087.

Lu, J., G. A. Vecchi, and T. Reichler, 2007: Expansion of the Hadley cell under global warming. *Geophys. Res. Lett.*, **34**, L06805, doi: 10.1029/2006GL028443.

Lunt, D. J., A. M. Haywood, G. A. Schmidt, U. Salzmann, P. J. Valdes, and H. J. Dowsett, 2010: Earth system sensitivity inferred from Pliocene modelling and data. *Nature Geoscience*, **3**, 60–64.

Maher, B. A., 2011: The magnetic properties of Quaternary aeolian dusts and sediments, and their palaeoclimatic significance. *Aeolian Research*, **3**, 87–144.

Pena-Ortiz, C., D. Gallego, P. Ribera, P. Ordonez, and M. D. C. Alvarez-Castro, 2013: Observed trends in the global jet stream characteristics during the second half of the 20th century. *J. Geophys. Res.*, **118**, 2702–2713.

Qiang, M., L. Lang, and Z. Wang, 2010: Do fine-grained components of loess indicate westerlies: Insights from observations of dust storm deposits at Lenghu (Qaidam Basin, China). *Journal of Arid Environments*, **74**, 1232–1239.

Rea, D. K., 1994: The paleoclimatic record provided by eolian deposition in the deep sea: The geologic history of wind. *Reviews of Geophysics*, **32**, 159–195.

Rea, D. K., and T. R. Janecek, 1982: Late Cenozoic changes in atmospheric circulation deduced from North Pacific eolian sediments. *Marine Geology*, **49**, 149–167.

Rea, D. K., and M. Leinen, 1988: Asian aridity and the zonal westerlies: Late Pleistocene and Holocene record of eolian deposition in the northwest Pacific Ocean. *Palaeogeography, Palaeoclimatology, Palaeoecology*, **66**, 1–8.

Rea, D. K., H. Snoeckx, and L. H. Joseph, 1998: Late Cenozoic eolian deposition in the North Pacific: Asian drying, Tibetan uplift, and cooling of the northern hemisphere. *Paleoceanography*, **13**, 215–224.

Rojas, M., 2013: Sensitivity of southern hemisphere circulation to LGM and $4 \times CO_2$ climates. *Geophys. Res. Lett.*, **40**, 965–970.

Rojas, M., and Coauthors, 2009: The southern westerlies during the last glacial maximum in PMIP2 simulations. *Climate Dyn.*, **32**, 525–548.

Rosenbloom, N. A., B. L. Otto-Bliesner, E. C. Brady, and P. J. Lawrence, 2013: Simulating the mid-Pliocene warm period with the CCSM4 model. *Geoscientific Model Development*, **6**, 549–561.

Salzmann, U., A. M. Haywood, D. J. Lunt, P. J. Valdes, and D. J. Hill, 2008: A new global biome reconstruction and data-model comparison for the middle Pliocene. *Global Ecology and Biogeography*, **17**, 432–447.

Seidel, D. J., Q. Fu, W. J. Randel, and T. J. Reichler, 2008: Widen-

ing of the tropical belt in a changing climate. *Nature Geoscience*, **1**, 21–24.

Sime, L. C., K. E. Kohfeld, C. Le Quéré, E. W. Wolff, A. M. de Boer, R. M. Graham, and L. Bopp, 2013: Southern hemisphere westerly wind changes during the last glacial maximum: Model-data comparison. *Quaternary Science Reviews*, **64**, 104–120.

Sloan, L. C., T. J. Crowley, and D. Pollard, 1996: Modeling of middle Pliocene climate with the NCAR GENESIS general circulation model. *Marine Micropaleontology*, **27**, 51–61.

Stepanek, C., and G. Lohmann, 2012: Modelling mid-Pliocene climate with COSMOS. *Geoscientific Model Development*, **5**, 1221–1243.

Sun, D. H., 2004: Monsoon and westerly circulation changes recorded in the late Cenozoic aeolian sequences of Northern China. *Global and Planetary Change*, **41**, 63–80.

Sun, D. H., R. X. Su, J. Bloemendal, and H. Y. Lu, 2008: Grain-size and accumulation rate records from Late Cenozoic aeolian sequences in northern China: Implications for variations in the East Asian winter monsoon and westerly atmospheric circulation. *Palaeogeography, Palaeoclimatology, Palaeoecology*, **264**, 39–53.

Sun, Y., G. Ramstein, C. Contoux, and T. J. Zhou, 2013: A comparative study of large-scale atmospheric circulation in the context of a future scenario (RCP4.5) and past warmth (mid-Pliocene). *Climate of the Past*, **9**, 1613–1627.

Taylor, K. E., 2001: Summarizing multiple aspects of model performance in a single diagram. *J. Geophys. Res.*, **106**, 7183–7192.

Thompson, R. S., and R. F. Fleming, 1996: Middle Pliocene vegetation: Reconstructions, paleoclimatic inferences, and boundary conditions for climate modeling. *Marine Micropaleontology*, **27**, 27–49.

Toggweiler, J. R., 2009: Shifting westerlies. *Science*, **323**, 1434–1435.

Toggweiler, J. R., J. L. Russell, and S. R. Carson, 2006: Midlatitude westerlies, atmospheric CO_2, and climate change during the ice ages. *Paleoceanography*, **21**, PA2005, doi: 10.1029/2005PA001154.

Wilcox, L. J., A. J. Charlton-Perez, and L. J. Gray, 2012: Trends in Austral jet position in ensembles of high-and low-top CMIP5 models. *J. Geophys. Res.*, **117**, D13115, doi: 10.1029/2012JD017597.

Yan, Q., Z. S. Zhang, H. J. Wang, D. B. Jiang, and W. P. Zheng, 2011: Simulation of sea surface temperature changes in the middle Pliocene warm period and comparison with reconstructions. *Chinese Science Bulletin*, **56**, 890–899.

Yan, Q., Z. S. Zhang, H. J. Wang, Y. Q. Gao, and W. P. Zheng, 2012: Set-up and preliminary results of mid-Pliocene climate simulations with CAM3.1. *Geoscientific Model Development*, **5**, 289–297.

Yin, J. H., 2005: A consistent poleward shift of the storm tracks in simulations of 21st century climate. *Geophys. Res. Lett.*, **32**, L18701, doi: 10.1029/2005GL023684.

Zhang, R., and Coauthors, 2013: Mid-Pliocene East Asian monsoon climate simulated in the PlioMIP. *Climate of the Past*, **9**, 2085–2099.

Zhang, R., and D. B. Jiang, 2014: Impact of vegetation feedback on the mid-Pliocene warm climate. *Adv. Atmos. Sci.*, **31**, 1407–1416, doi: 10.1007/s00376-014-4015-5.

Zhang, Z., and Q. Yan, 2012: Pre-industrial and mid-Pliocene simulations with NorESM-L: AGCM simulations. *Geoscientific Model Development*, **5**, 1033–1043.

Zhang, Z. S., and Coauthors, 2012: Pre-industrial and mid-Pliocene simulations with NorESM-L. *Geoscientific Model Development*, **5**, 523–533.